

Fully spin-dependent transport of triangular graphene flakes

Tomoya Ono¹, Tadashi Ota¹, and Yoshiyuki Egami²

¹*Department of Precision Science and Technology,*

Osaka University, Suita, Osaka 565-0871, Japan

²*Nagasaki University Advanced Computing Center,*

Nagasaki University, Bunkyo-machi, Nagasaki 852-8521, Japan

(Dated: November 18, 2018)

Abstract

The magnetic moment and spin-polarized electron transport properties of triangular graphene flakes surrounded by boron nitride sheets (BNC structures) are studied by first-principles calculation based on density functional theory. Their dependence on the BNC structure is discussed, revealing that small graphene flakes surrounded by large BN segments have a large magnetic moment. When the BNC structure is suspended between graphene electrodes, the spin-polarized charge density distribution accumulates at the edge of the graphene flakes and no spin polarization is observed in the graphene electrodes. We also found that the BNC structure exhibits perfectly spin-polarized transport properties in a wide energy window around the Fermi level. Our first-principles results indicate that the BNC structure provides for the new possibilities for the electrical control of spin.

⁸ PACS numbers: 72.80.Vp, 73.21.-b, 75.75.-c, 85.75.Mm

9 I. INTRODUCTION

10 Graphene,¹ a two-dimensional monolayer honeycomb structure of carbon, is known to
11 exhibit a rich variety of electronic structures and is one of the most promising new materials
12 for future nanoelectronics. The electronic reconstruction of graphenes induced at boundaries
13 can give rise to metal or insulator states,² magnetism,³ or even superconductivity.⁴ The
14 discovery of zigzag graphene nanoribbons,^{3,5} in which an opposite spin orientation crosses
15 the ribbon between ferromagnetically ordered edge states on each edge, through theoretical
16 calculations has attracted a great deal of interest^{6,7} in spintronics applications based on
17 graphene-based materials. The possibility of controlling electron transport by means of
18 the spin degree of freedom has recently attracted attention, because spintronics devices
19 may have potential for applications in future commercial electronics and for generating
20 insights into the fundamental properties of electron spin in solids. From the viewpoint
21 of the development of highly efficient spintronics devices, the spin-filter effect, which can
22 be used for the efficient injection of spins into magnetic junctions, is an important issue of
23 concern and debate. Okada and Oshiyama⁸ studied the spin polarizations of two-dimensional
24 structures composed of boron, nitrogen, and carbon, in which triangular graphene flakes are
25 surrounded by boron nitride (BN) sheets (referred to as BNC structures hereafter), through
26 first-principles calculations and found that flat-band states can be observed around the Fermi
27 level and the BNC structures are ferromagnetically polarized. Zheng *et al.*⁹ examined the
28 spin transport properties of graphene antidots, i.e., graphenes with rectangular or triangular
29 holes, and observed the spin polarization of electron current in triangular antidots. However,
30 the energy window where current is perfectly spin-polarized is rather small in their system
31 because the energy of the edge states contributing to spin-polarized current does not shift
32 significantly around the antidots.

33 We study the relationship between the magnetic moment of BNC structures and their
34 sizes. The spin-dependent transport properties of graphene/BNC/graphene (G/BNC/G)
35 structures, where BNC structures are sandwiched with graphene electrodes, are also ex-
36 amined. We found that small graphene flakes surrounded by long BN segments exhibit
37 a large magnetic moment and that the BNC structures with small flakes exhibit a fully
38 spin-polarized current with a large energy range of the incident electrons.

39 All calculations are done within the framework of density functional theory (DFT)¹⁰

40 using a real-space finite-difference approach,^{11,12} which makes it possible to carry out cal-
 41 culations with a high degree of accuracy by combining them with a timesaving double-
 42 grid technique.^{12,13} Valence electron-ion interaction is described using norm-conserving
 43 pseudopotentials¹⁴ generated by the scheme proposed by Troullier and Martins.¹⁵ Exchange
 44 and correlation effects are treated within the local spin density approximation¹⁶ of DFT.

45 II. RESULTS AND DISCUSSION

46 A. Magnetic moment of graphene flakes

47 Let us first consider three periodic BNC structures to investigate the effect of the size
 48 of carbon regions on the magnetic moment. Figures 1(a), 1(b), and 1(c) show the compu-
 49 tational models we employed here. Here and hereafter, we refer to the BNC structures in
 50 Figs. 1(a), 1(b), and 1(c) as models 1(a), 1(b), and 1(c), respectively. There are 64 atoms in
 51 the supercell. Periodic boundary conditions are imposed on all directions, and a repeating
 52 sheet model is separated by 9.0 \AA in each layer for all calculations presented in this section.
 53 The Brillouin zone is sampled using a $2 \times 1 \times 8$ k -point grid. The lattice constant of graphene
 54 is set at 1.41 \AA with a real-space grid spacing of $\sim 0.18 \text{ \AA}$, and structural optimization is per-
 55 formed until the remaining forces are less than 5 mRy/\AA . The calculated magnetic moments
 56 of the BNC structures are listed in Table I. In addition, the electronic band structures are
 57 plotted in the middle panels of Fig. 1. The magnetic moment of the BNC structures with
 58 the large graphene flakes [models 1(a) and 1(b)] are zero, and the moment becomes $S_0=2$, as
 59 expected from Lieb's theorem for a biparticle lattice,¹⁷ when the graphene segment becomes
 60 small. We then examine variations in the magnetic moments as a function of the distance
 61 in the z direction between graphene flakes in the neighboring supercell. Figures 2(a), 2(b),
 62 2(c), and 2(d) show the calculated atomic configurations. Integration over the Brillouin zone
 63 is carried out using a $4 \times 1 \times 8$ k -point grid. The calculated magnetic moments and electronic
 64 band structures are shown in Table I and in the middle panels of Fig. 2, respectively. No
 65 spin polarization is observed in the BNC structure with the shortest graphene-flake distance
 66 [model 2(a)]. The magnetic moment increases with increasing in the graphene-flake distance
 67 because the BN regions insulate the triangular flakes so that the behavior of the edge states
 68 is flat. The moment S_0 approaches a noninteger value of ~ 1.5 and does not become 2.0

69 since the energy bands of the edge states deviate along the x direction in the Brillouin zone.
 70 The bottom panels of Figs. 1 and 2 also show the calculated spin densities, $n_{\uparrow}(r) - n_{\downarrow}(r)$,
 71 of the BNC structures. One can see that magnetic ordering appears on the edge of the
 72 graphene flakes and that the magnetic moment is strengthened when the electrons around
 73 the graphene flakes are localized by the insulating behavior of the BN regions.

74 We then investigate the reason of the absence of magnetic ordering in models 1(a), 1(b),
 75 and 2(a). In studies on metallic magnetism, the Stoner condition provides a natural starting
 76 point, $I(E_F) \cdot \text{DOS}(E_F) > 1$, where $I(E_F)$ is called the Stoner parameter¹⁸ and DOS is
 77 the density of states at the Fermi level, which are computed in the spin-unpolarized limit.
 78 The values of $I(E_F) \cdot \text{DOS}(E_F)$ are 0.29, 0.58, and 1.23 for models 1(a), 1(b), and 1(c),
 79 respectively. In model 1(c), the energy bands of the edge states of the graphene flakes,
 80 which play an important in the ferromagnetic ordering, do not vary significantly in the
 81 Brillouin zone, and the DOS at the Fermi energy is high. In contrast, the energy bands
 82 around the Fermi level are dispersive in models 1(a) and 1(b) owing to the metallic property
 83 of the graphene sheet, which results in a spin-unpolarized ground-state electronic structure.
 84 On the other hand, the reason for the absence of the magnetic moment in model 2(a) is
 85 different from that for Fig. 1. Since the BN segment is not sufficiently large in model 2(a),
 86 the two energy bands around the Fermi level are separated energetically, and a high DOS
 87 at the Fermi level is not observed.

88 **B. Magnetic moment of G/BNC/G structure**

89 Graphene is one of the best candidates for buffer layers between BNC structures and
 90 electrodes because of its metallic characteristics and long-lived spin coherence. We explore
 91 the magnetic moment of BNC structures connected to graphene (G/BNC/G structures).
 92 Since the transition from ferromagnetic to nonmagnetic states occurs when fewer than 0.05
 93 electrons are doped per BNC structure and the existence of an optimum width for the BN
 94 region has been given,⁸ it is of interest whether ferromagnetic states can still be observed
 95 in G/BNC/G structures. When primary importance is attached to the magnetic moment
 96 of BNC structures, a wider BN region is necessary to obtain a large magnetic moment.
 97 However, in terms of the transmission of electrons, a wider BN region acting as an insulator
 98 could be an obstacle to obtaining larger conductance. The computational models used to

99 investigate the magnetic moment are outlined in Fig. 3. The integration over the Brillouin
100 zone for the x direction is carried out by equidistant sampling of the four k -point grid. The
101 calculated total magnetic moments are found to be 1.51 and 1.62 μ_B/cell for models 3(a) and
102 3(b), respectively. The magnetic behavior is illustrated by plotting contours of the difference
103 in the charge density distributions on the plane in Fig. 3. Note that the spin polarization
104 accumulates in the BNC regions and that the graphene structures as the electrodes do not
105 exhibit magnetic ordering.

106 C. Transport properties of G/BNC/G structure

107 It is important to evaluate quantitative spin transmissions toward the application of
108 spin-filter materials. Based on the results in the previous subsection, the spin-transport
109 properties of models 3(a) and 3(b) are investigated. We establish a computational model
110 for the transport calculations, where the G/BNC/G structures are sandwiched between
111 electrodes. Hereafter, we refer to the G/BNC/G structures in Figs. 3(a) and 3(b) connected
112 to *semi-infinite* graphene electrodes as models A and B, respectively. The scattering wave
113 functions of the electrons propagating from the left electrode are determined to include the
114 rest of the semi-infinite electrodes by solving the following simultaneous equations for each
115 incident wave function $\Phi_L^{in}(z_k)$:

$$\left[E - \hat{H}_T - \hat{H}_\Sigma \right] \begin{bmatrix} \Psi(z_0) \\ \Psi(z_1) \\ \vdots \\ \Psi(z_{N_z+1}) \end{bmatrix} = \begin{bmatrix} B_z^\dagger \Phi_L^{in}(z_{-1}) - \Sigma_L^r(z_0) \Phi_L^{in}(z_0) \\ 0 \\ \vdots \\ 0 \end{bmatrix}. \quad (1)$$

116 Here, \hat{H}_T is the truncated part of the Hamiltonian of the scattering region and E is the
117 energy of the incident electrons. $\Psi(z_i)$ is the set of values of the scattering wave function on
118 the x - y plane at $z = z_i$ and it satisfies the scattering boundary condition, i.e.,

$$\Psi(z_k) = \begin{cases} \Phi_L^{in}(z_k) + \sum_{i=1}^{N_x N_y} r_i \Phi_i^{ref}(z_k) & (k \leq 0) \\ \sum_{i=1}^{N_x N_y} t_i \Phi_i^{tra}(z_k) & (k \geq N_z + 1) \end{cases}, \quad (2)$$

119 where r_i (t_i) is the reflection (transmission) coefficient, $\Phi_i^{ref}(z_k)$ ($\Phi_i^{tra}(z_k)$) is the generalized
120 Bloch state in the semi-infinite electrodes for reflected (transmitted) electrons, and N_x , N_y ,

121 and N_z are the numbers of grid points in the x , y , and z directions, respectively. In addition,
 122 \hat{H}_Σ is a zero matrix except for the first and the last elements, which are the retarded self-
 123 energy matrices for the left and right electrodes, $\Sigma_L^r(z_0)$ and $\Sigma_R^r(z_{N_z+1})$, respectively. Further
 124 details can be found in Refs. 19 and 20. The retarded self-energy matrices for the graphene
 125 electrodes are employed, and eight graphene buffer layers are inserted between the BNC
 126 structure and electrodes. A grid spacing of 0.21 Å is employed. The scattering wave
 127 functions from the right electrode are treated in the same way. We first calculate \hat{H}_T using
 128 periodic boundary conditions and then compute the scattering wave functions obtained
 129 non-self-consistently. It has been reported that this procedure is just as accurate as fully
 130 self-consistent calculations in the linear response regime but significantly more efficient than
 131 being self-consistent on a scattering basis.²¹ The Brillouin zone is sampled with the four
 132 k -point grid to set up \hat{H}_T . The conductance per unit cell under zero temperature and zero
 133 bias is described by the Landauer-Büttiker formula,²²

$$G(E) = G_0 \int d\mathbf{k}_\parallel \frac{A}{(2\pi)^2} \text{Tr}(\mathbf{T}^\dagger \mathbf{T}), \quad (3)$$

134 where \mathbf{T} is a transmission-coefficient matrix, A is the area of the unit cell in the x and y
 135 directions, and $G_0 = 2e^2/h$ with e and h being the electron charge and Planck's constant,
 136 respectively.

137 Figure 4 plots the conductance of G/BNC/G structures as a function of the energy of the
 138 incident electrons. Although BN sheets are insulators, considerable electron transmission
 139 through BNC structures can be observed. The magnitude of conductance for model B is
 140 smaller than that for model A because of the insulating behavior of the long BN regions.
 141 In addition, the conductance spectrum of model B contains sharp peaks attributed to the
 142 resonant tunneling. There is a significant spin-polarized electron current observed that can
 143 be associated with the BNC structures. Here, we define the parameter $P(E) = [\sigma_\uparrow(E) -$
 144 $\sigma_\downarrow(E)]/[\sigma_\uparrow(E) + \sigma_\downarrow(E)]$ to characterize the spin polarization of electron current, where the
 145 conductance of spin $s(=\uparrow, \downarrow)$ is denoted by $\sigma_s(E)$. The spin-polarization ratio is found to
 146 be ~ 1 , which is comparable to that obtained with ferromagnetic tunnel junctions using a
 147 transition metal.²³ The peaks of the conductance of the up-spin and down-spin channels are
 148 split by ~ 0.5 eV. The differences between the positions of the peaks for the up-spin and
 149 down-spin spectra are similar for models A and B because the splitting of the bands for the
 150 up-spin and down-spin edge states is almost equal in Figs. 3(c) and 3(d). Moreover, the

151 energy ranges of $P(E) = 1$ and those of $P(E) = -1$ are completely separated. Although
 152 graphene is a gapless semiconductor, the conductance of the up spin (down spin) is negligibly
 153 small except for in the energy ranges of $P(E) = 1$ ($P(E) = -1$) because of the finite size
 154 effect of the triangular flakes surrounded by the BN sheets. This means that we can control
 155 the spin-polarized current by tuning the gate bias.

156 Figure 5 shows the local density of states (LDOS) of model B, which is plotted by in-
 157 tegrating them along the x - y plane, $\rho(z, E) = \int |\psi(\mathbf{r}, E)|^2 d\mathbf{r}_{\parallel}$, where $\mathbf{r} = (x, y, z)$, ψ is
 158 the wave function, and E is the energy of the states. The states of up-spin electrons are
 159 shifted to lower energies and those of down-spin electrons are shifted to higher energies in
 160 the BNC structure, although the spin polarization is negligibly small in the LDOS of the
 161 graphene region. Thus, the conductance spectrum of the BNC structure is not symmetric
 162 around the Fermi level, whereas that for graphene is symmetric. Moreover, the difference
 163 in energy between these states of up-spin and down-spin electrons is ~ 0.5 eV. We can see
 164 good correspondence between the conductance and LDOS, which implies that the electronic
 165 structure of the BNC structure contributes to the spin-polarized electron current.

166 To investigate the origin of the two significant peaks in the conductance spectrum in
 167 Fig. 4(b), we show in Fig. 6 the charge density distribution of scattering waves for model B,
 168 in which the distribution of the waves for incident electrons from the left electrode is plotted.
 169 In Fig. 7, the charge density distribution of the two edge states around the Fermi level in
 170 model 2(c) is also depicted. The charge density distribution of the energetically lower edge
 171 state [indicated by α in Fig. 2(c)] is aligned along a slope of the triangular graphene flake
 172 and that of the higher edge state [indicated by β] is parallel to the base. As can be seen in
 173 Fig. 6, the lower edge state contributes to electron transport at low energies and the higher
 174 edge state contributes to electron transport at high energies in both spin channels.

175 Such a spintronic device can be compared to another theoretical proposal that achieves
 176 a spin-filter material. Compared with the graphene antidot system,⁹ this BNC structure
 177 has a wider energy window where the current is fully polarized. The inserted BN segment
 178 between the graphene flakes and electrodes insulates the edge states so that the edge states
 179 accumulate in the graphene flakes, which results in a higher magnetic moment for the BNC
 180 structure. Our results indicate that the BNC structure is one of the most promising candi-
 181 dates for electronic control over spin transport.

182 **III. SUMMARY**

183 We investigated the electronic structures and transport properties of triangular graphene
184 flakes surrounded by BN sheets using first-principles calculations. We found that the mag-
185 netic moment of the graphene flakes increases as the flakes become small and as they are
186 surrounded by a large BN region. When the BNC structure is connected to graphene elec-
187 trodes, the spin polarization of the charge density distribution accumulates at the edges of
188 the flakes and no spin polarizations is observed in the graphene electrodes. First-principles
189 transport calculation revealed that electron transport through the BNC structure is fully
190 polarized in a wide energy range around the Fermi level. These results should stimulate
191 interest in spin-transport devices using carbon-based materials and bottom-up technology.

192 **ACKNOWLEDGEMENTS**

193 The authors would like to thank Kikuji Hirose and Yoshitada Morikawa of Osaka Uni-
194 versity for fruitful discussion. This research was partially supported by Strategic Japanese-
195 German Cooperative Program from Japan Science and Technology Agency and Deutsche
196 Forschungsgemeinschaft, by a Grant-in-Aid for Scientific Research on Innovative Areas
197 (Grant No. 22104007) from the Ministry of Education, Culture, Sports, Science and Tech-
198 nology, Japan. The numerical calculation was carried out using the computer facilities of
199 the Institute for Solid State Physics at the University of Tokyo, the Research Center for
200 Computational Science at the National Institute of Natural Science, Center for Computa-
201 tional Sciences at University of Tsukuba, and the Information Synergy Center at Tohoku
202 University.

203 ¹ K.S. Novoselov, A.K. Geim, S.V. Morozov, D. Jiang, Y. Zhang, S.V. Dubonos, I.V. Grigorieva,
204 and A.A. Firsov, *Science* **306**, 666 (2004).

205 ² N. Hamada, S.I. Sawada, and A. Oshiyama, *Phys. Rev. Lett.* **68**, 1579 (1992).

206 ³ M. Fujita, K. Wakabayashi, K. Nakada and K. Kusakabe, *J. Phys. Soc. Jpn.* **65**, 1920 (1996).

207 ⁴ H.B. Heersche, P. Jarillo-Herrero, J.B. Oostinga, L.M.K. Vandersypen, and A.F. Morpurgo,
208 *Nature* **446**, 56 (2007).

- 209 ⁵ K. Nakada, M. Fujita, G. Dresselhaus, and M.S. Dresselhaus, Phys. Rev. B **54**, 17954 (1996).
- 210 ⁶ N. Tombros, C. Jozsa, M. Popinciuc, H.T. Jonkman, and B.J. van Wees, Nature **448**, 571
211 (2007).
- 212 ⁷ V.M. Karpan, G. Giovannetti, P.A. Khomyakov, M. Talanana, A.A. Starikov, M. Zwierzycki,
213 J. van den Brink, G. Brocks, and P.J. Kelly, Phys. Rev. Lett. **99**, 176602 (2007).
- 214 ⁸ S. Okada and A. Oshiyama, Phys. Rev. Lett. **87**, 146803 (2001).
- 215 ⁹ X.H. Zheng, G.R. Zhang, Z. Zeng, Víctor M. García-Suárez, and Colin J. Lambert, Phys. Rev.
216 B **80**, 075413 (2009).
- 217 ¹⁰ P. Hohenberg and W. Kohn, Phys. Rev. **136**, B864 (1964).
- 218 ¹¹ J.R. Chelikowsky, N. Troullier, and Y. Saad, Phys. Rev. Lett. **72**, 1240 (1994)
- 219 ¹² K. Hirose, T. Ono, Y. Fujimoto, and S. Tsukamoto, *First Principles Calculations in Real-Space*
220 *Formalism, Electronic Configurations and Transport Properties of Nanostructures* (Imperial
221 College, London, 2005).
- 222 ¹³ T. Ono and K. Hirose, Phys. Rev. Lett. **82**, 5016 (1999); Phys. Rev. B **72**, 085115 (2005).
- 223 ¹⁴ We used the norm-conserving pseudopotentials NCPS97 constructed by K. Kobayashi. See K.
224 Kobayashi, Comput. Mater. Sci. **14**, 72 (1999).
- 225 ¹⁵ N. Troullier and J. L. Martins, Phys. Rev. B **43**, 1993 (1991).
- 226 ¹⁶ J. P. Perdew and A. Zunger, Phys. Rev. B **23**, 5048 (1981).
- 227 ¹⁷ E.H. Lieb, Phys. Rev. Lett. **62**, 1201 (1989).
- 228 ¹⁸ J.F. Janak, Phys. Rev. B **16**, 255 (1977); M.M. Sigalas and D.A. Papaconstantopoulos, Phys.
229 Rev. B **50**, 7255 (1994).
- 230 ¹⁹ Y. Fujimoto and K. Hirose, Phys. Rev. B **67**, 195315 (2003).
- 231 ²⁰ L. Kong, M.L. Tiago, and J.R. Chelikowsky, Phys. Rev. B **73**, 195118 (2006).
- 232 ²¹ L. Kong, J.R. Chelikowsky, J.B. Neaton, and Steven G. Louie, Phys. Rev. B **76**, 235422 (2007).
- 233 ²² M. Büttiker, Y. Imry, R. Landauer, and S. Pinhas, Phys. Rev. B **31**, 6207 (1985).
- 234 ²³ S. Kokado, N. Fujima, K. Harigaya, H. Shimizu, and A. Sakuma, Phys. Rev. B **73**, 172410
235 (2006).

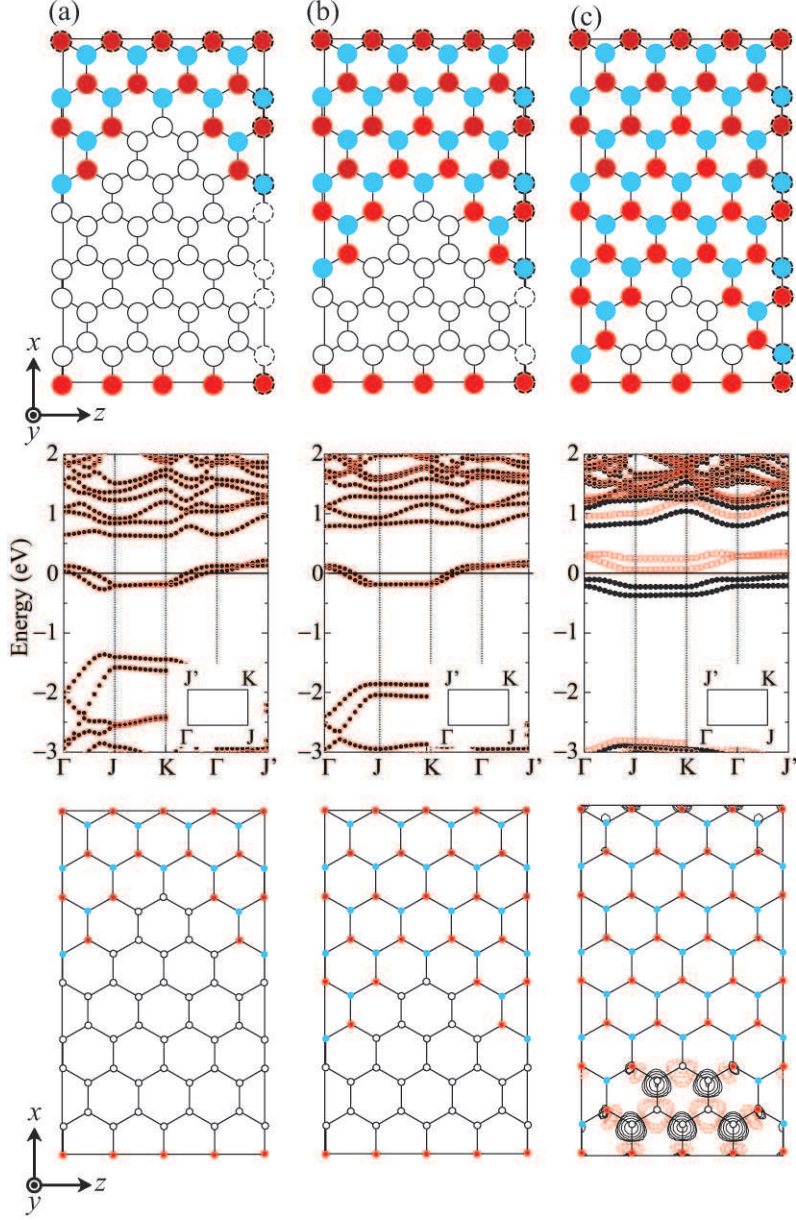


FIG. 1. (color online) Top view of computational models (top panel), electronic band structures (middle panel), and contour plots showing difference between up-spin and down-spin charge density distributions (bottom panel). (a) represents a large graphene flake model, (b) represents a medium graphene flake model, and (c) represents a small graphene flake model. White, light blue (gray), and red (black) circles correspond to C, B, and N atoms. The atoms enclosed by dashed circles are in the neighboring supercell. In the band structures, closed and open circles are up-spin and down-spin bands, respectively. In the contour plots, positive values of spin density are indicated by solid lines and negative values by dashed lines. Each contour represents twice or half the density of the adjacent contour lines. The lowest contour represents $3.29 \times 10^{-3} e/\text{\AA}^3$.

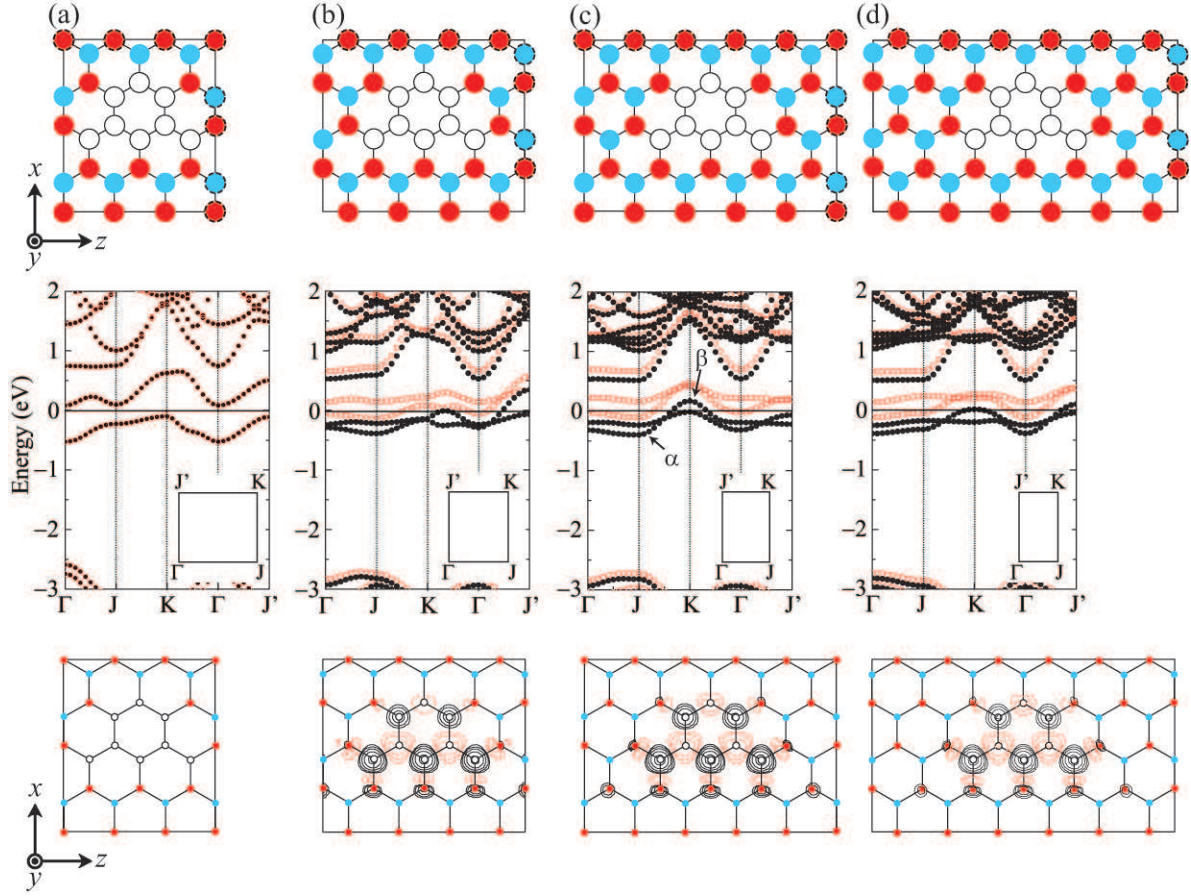


FIG. 2. (color online) Top view of computational models (top panel), electronic band structures (middle panel), and contour plots showing difference between up-spin and down-spin charge density distributions (bottom panel). (a), (b), (c), and (d) correspond to short, medium, long, and very long distances between graphene flakes. The symbols have the same meanings as those in Fig. 1.

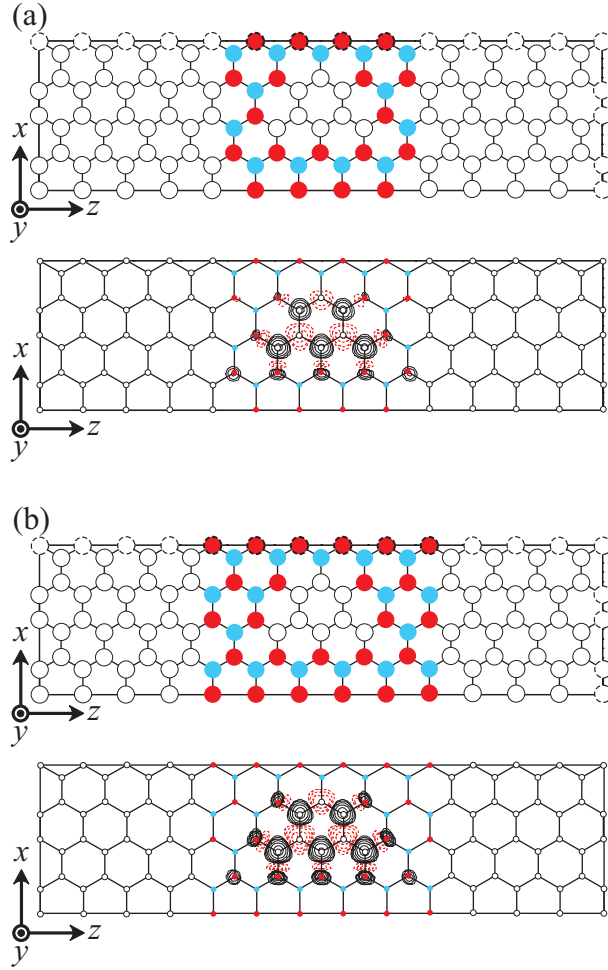


FIG. 3. (color online) Top view of computational models (top panel) and contour plots showing difference between up-spin and down-spin charge density distributions (bottom panel). The symbols have the same meanings as those in Fig. 1.

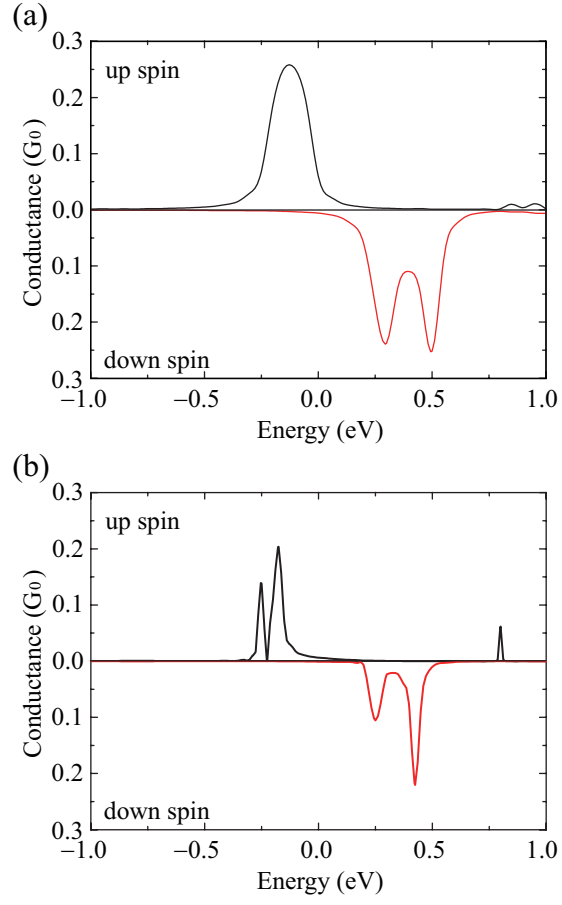


FIG. 4. (color online) Conductance as a function of energy of incident electrons. Zero energy is chosen to be at the Fermi level.

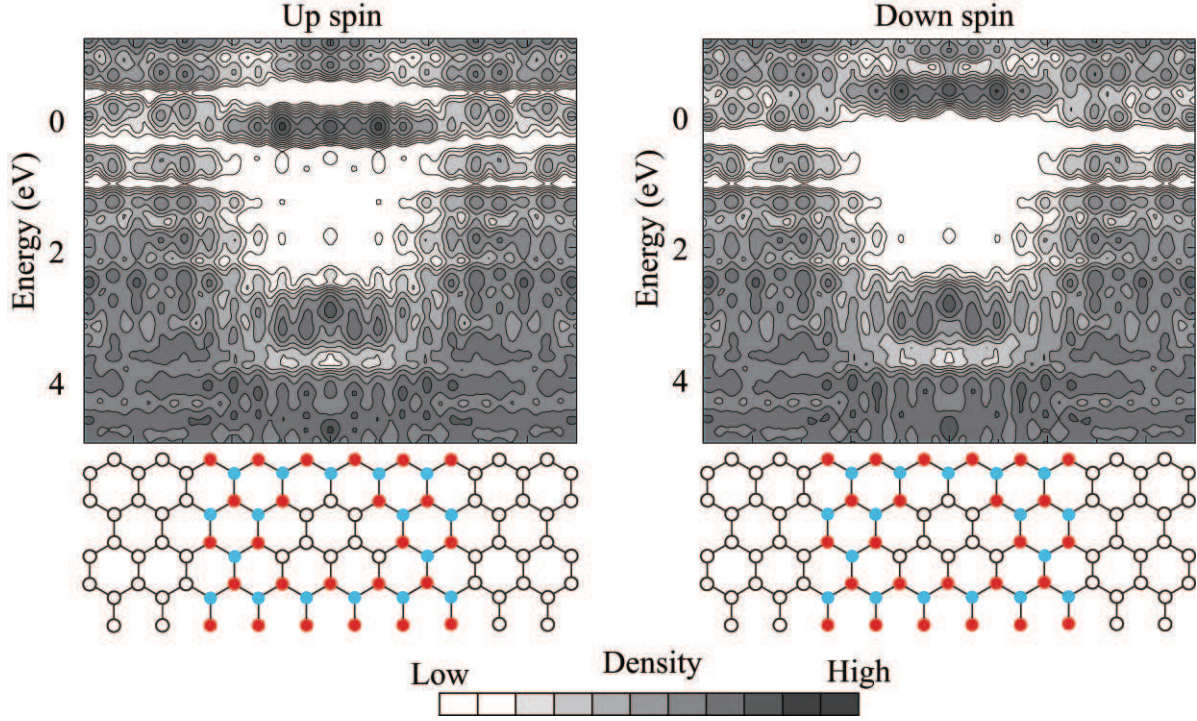


FIG. 5. (color online) Distributions of LDOS of G/BNC/G structure integrated on plane parallel to interface as functions of relative energy from Fermi level. Zero energy is chosen to be at the Fermi level. Each contour represents twice or half the density of the adjacent contour lines, and the lowest contour is $6.78 \times 10^{-5} e/eV/\text{\AA}$. The atomic configurations are given as a visual guide below the graph, and the symbols have the same meanings as those in Fig. 1.

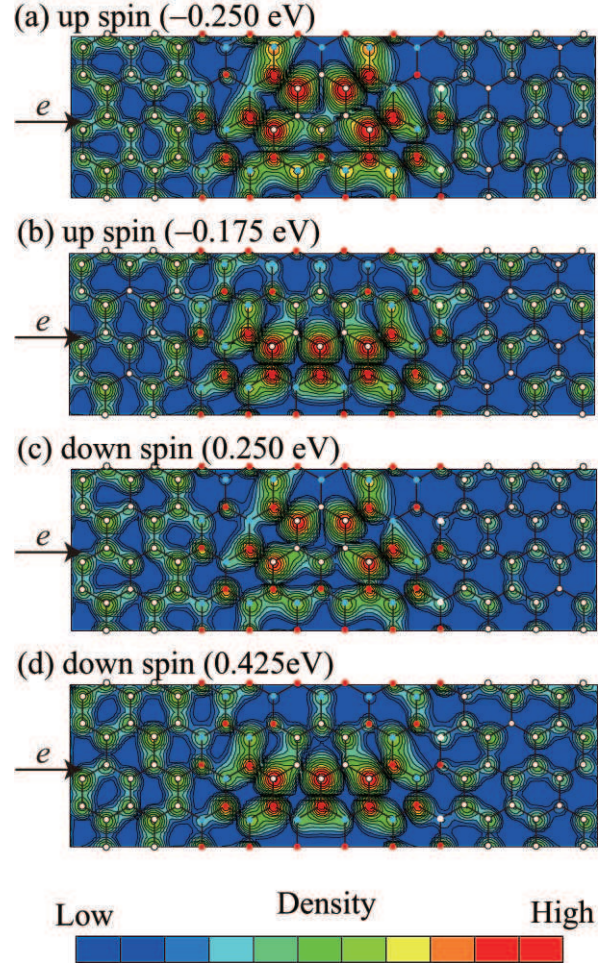


FIG. 6. (color) Charge density distributions of scattering waves for incident electrons emitted from left electrode on plane parallel to BNC structure of model B. Each contour represents twice or half the density of the adjacent contour lines, and the lowest contour is $1.96 \times 10^{-3} e/eV/\text{\AA}^3$. The symbols have the same meanings as those in Fig. 1. Energies in parentheses are relative to the Fermi level.

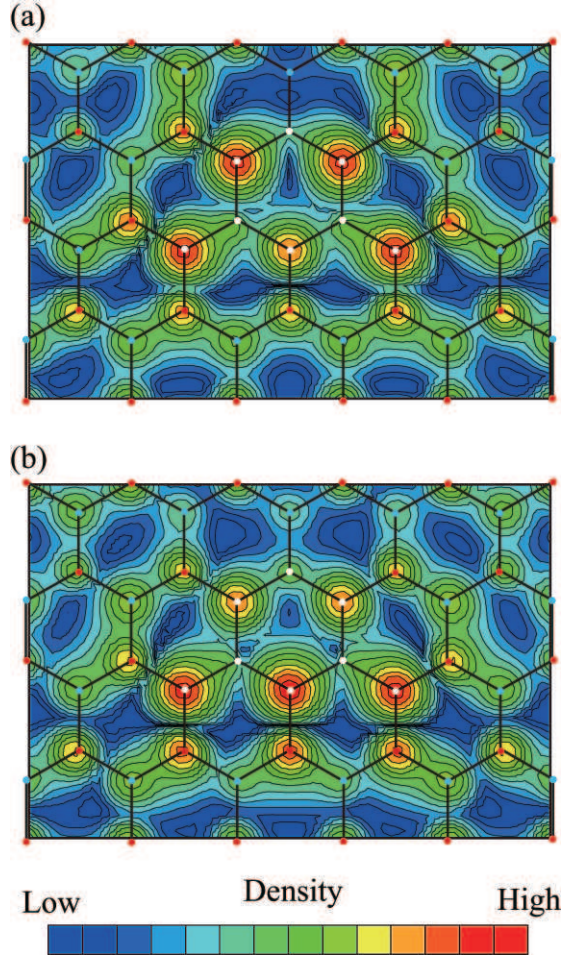


FIG. 7. (color) Charge density distributions of (a) lower edge state [indicated by α] and (b) higher edge state [indicated by β] around the Fermi level for BNC structure in Fig. 2(c). Each contour represents twice or half the density of the adjacent contour lines, and the lowest contour is $1.29 \times 10^{-5} e/\text{\AA}^3$.

238 **TABLES**

239

TABLE I. Calculated magnetic moments of BNC structures. 1(a), 1(b), 1(c), 2(a), 2(b), 2(c), and 2(d) correspond to structures in Figs. 1 and 2.

Model	Magnetic moment (μ_B/cell)
1(a)	0.00
1(b)	0.00
1(c)	2.00
2(a)	0.00
2(b)	1.39
2(c)	1.44
2(d)	1.46